European Journal of Mechanics / A Solids 72 (2018) 148–154

Contents lists available at ScienceDirect

European Journal of Mechanics / A Solids

journal homepage: www.elsevier.com/locate/ejmsol

On the diametric compression strength test of brittle spherical particles

Goran Žagar*, Václav Pejchal, Marc Kissling, Andreas Mortensen

Laboratory of Mechanical Metallurgy, Institute of Materials, École Polytechnique Fédérale de Lausanne (EPFL), Station 12, CH-1015 Lausanne, Switzerland

ARTICLE INFO

Keywords:
Diametric compression
Spherical particles
FE analysis
Local strength

ABSTRACT

Diametric compression testing can be used to measure the hoop strength of spherical particles if one uses platens whose deformation behaviour is tailored in a way that allows the particles to sink sufficiently far into the platens before particle fracture takes place. To obtain the hoop stress of a compressed spherical particle at the moment of failure, and thus interpret the strength tests, an analytical solution derived by Hiramatsu and Oka is generally used. In deriving their analytical equations, Hiramatsu and Oka assumed that the contact stress between the spherical particle and the platens is radial and uniform along two equal diametrically opposed spherical caps.

Here we revisit, by means of the finite element method, the mechanics that underlie the diametrical compression of a linear elastic sphere between two parallel and planar elasto-plastic platens. We show that the Hiramatsu and Oka equations give valid hoop stress values only when the contact area between the compressed sphere and the platens is less than roughly 5% of the equatorial sphere cross-sectional area. At higher contact areas, when the spheres are more deeply embedded in the platen material and the test can be used to measure the particle hoop strength, the Hiramatsu and Oka solution underestimates the hoop stress. By conducting a parametric study, we provide simple expressions that can be used to quickly, yet accurately to within the , compute the hoop stress of compressed spheres in diametric compression tests as a function of the contact area knowing only two parameters, namely the Poisson's ratio of the material making the sphere and the sphere/platen contact friction coefficient.

1. Introduction

The diametric compression of a sphere between two parallel platens is a mechanical problem that is frequently encountered, notably in the context of particle compression testing. This test is often used to measure the fracture strength of particles, something that is made possible because there are regions in a sphere compressed between two parallel platens that are subjected to tensile stress; these regions are situated notably in the particle center and along its outer ”equatorial” surface, where the sphere surface is roughly normal to the platens.

Given its practical importance, the compression of a sphere between two parallel platens is a problem that has been extensively investigated. The most frequently used result is the stress field distribution derived analytically for a linear-elastic isotropic sphere, of Poisson's ratio ν_s and radius R, that is diametrically compressed by a uniformly distributed normal (i.e., radial) pressure p acting over two equal and opposite spherical caps of circular periphery having radius a. The solution to this problem was derived by Hiramatsu and Oka (Hiramatsu and Oka, 1966, 1967; Salençon, 1966), and similarly before them, by Sternberg and Rosental (Sternberg and Rosenthal, 1952) and Dean et al. (1952). The stress field equations for the sphere are written in spherical coordinates, (r, θ, ϕ), in terms of infinite Fourier-Legendre series.

The Hiramatsu and Oka solution is highly relevant to particle compression testing because it provides a theoretical basis for a simple expression that is often used to compute the (tensile) ”strength”, σ_T, of tested individual particles, namely $\sigma_T = \kappa F_c/\pi R^2$ where F_c is the applied compressive load at the onset of particle failure, and κ is a proportionality factor of order of magnitude 1 (Zhao et al., 2013; Aman et al., 2010; Antonyuk et al., 2005; Chau and Wei, 1999; Gerberich et al., 2003; Huang et al., 2014; Jaeger, 1967; Mcdowell and Amon, 2000; McDowell and Bolton, 1998; Mook et al., 2007; Ogiso et al., 2007; Pitchumani et al., 2004; Portnikov et al., 2013; Ribas et al., 2014; Rozenblat et al., 2011; Wijk, 1978; Yap et al., 2008; Yoshida et al., 2005; Zhao et al., 2013). Use of this expression is justified by the fact that in particle compression testing, one typically utilizes flat and stiff platens that are much harder than the particles themselves (typically, diamond is used). As a consequence, the relative contact radii, a/R, observed in such experiments are well below unity, since hard platens prevent sinking-in of particles into the platens. Hiramatsu and Oka's equations show then that, for $a/R \leq 0.13$, the maximum (tensile) first principal stress likely to cause fracture of brittle spherical particles is located within the sphere along its loading axis (the line linking the

* Corresponding author.
E-mail address: gorzagar@gmail.com (G. Žagar).

https://doi.org/10.1016/j.euromechsol.2018.04.016
Received 11 March 2018; Accepted 25 April 2018
Available online 02 May 2018

center of the two load application areas), and is given by the above equation with $\kappa \approx 0.7$. The exact magnitude of this peak tensile stress, ($\kappa F_c/\pi R^2$ or in other words of κ), besides being sensitive to the Poisson's ratio of the particle, varies also with a/R.

Use of this expression in particle compression testing has been debated extensively, to question why particles should break starting from their center, or to question what value one should assign to the proportionality factor κ (Darvell, 1990). Often κ is simplified to a constant of value between ≈ 0.2 and ≈ 1.4, with no agreement to date on what (single) value one should use. In addition, the physical significance of the entire test has been questioned because brittle particles that fail under compression at small a/R often do so, not starting at a preexisting flaw, but due to the nucleation and growth of extraneous cracks along the ring of high stress concentration that appears just outside the perimeter of particle–platen contacts when very hard platens are used (Schönert, 2004; Swab et al., 2011; Khanal et al., 2005; Tang et al., 2001; Chen et al., 2007; Mazel et al., 2016).

This led Shipway and Hutchings, 1993a, 1993b to revisit the test and propose a new approach, which is to measure the strength of compressed particles at high contact radii (a/R up to ≈ 0.8). Advantages of doing so are first that stress concentration along the periphery of platen/particle contact is eliminated (thus eliminating the formation of extraneous flaws there), and secondly that for sufficiently high a/R, the location of peak tensile first principal stress in a compressed sphere shifts away from the interior of the sphere and becomes located along its equator. To obtain such high contact radii, relatively soft elasto-plastic platens need to be used, implying that one should allow significant embedding of the particles into the platens prior to their failure. The approach proposed by Shipway and Hutchings was recently used and extended by Pejchal et al. (2017) to produce statistical measures of the surface strength of microscopic fused quartz particles. In that work, spherical particles were compressed up to the point of failure using four different steel platens of tailored hardness. The hoop strength of the fused quartz particles was evaluated at a/R in the range from ≈ 0.65 to ≈ 0.8 using the Hiramatsu and Oka equations, based on values at the moment of failure for each particle of the "critical" force, F_c, and of the "critical" relative contact radius (measured by observation of the plastic imprint left along the platen surface by the particle as it embedded into the platen), a_c/R. Data were treated using the theory of survival analysis to derive estimates of the particle strength distribution as governed by their surface flaws.

At high values of a/R, however, use of the Hiramatsu and Oka equations becomes questionable, notably because it is likely that the nature of the contact stress distribution deviates from the uniform and normal distribution assumed in their analysis. In preliminary work, by modeling the compression of a fused quartz particle and explicitly including steel-like elasto-plastic platens in a finite element model, Pejchal et al. noted that Hiramatsu and Oka equations captured very well the hoop stress of a sphere at small a/R. At high a/R values, where the particle strength is measured in this newer approach to particle compression testing, the Hiramatsu and Oka equations on the other hand significantly underestimate the hoop stress of the sphere (at $a/R \approx 0.8$ the underestimation is $\approx 30\%$). This discrepancy is mainly rationalized on the ground that, with increasing a/R, the contact stress between the platens and the sphere increasingly deviates from being uniform and purely normal to the contact surface, which is in contrast to what Hiramatsu and Oka equations assume. To provide values for the stress in the sphere's center and along the sphere's equator under more realistic test conditions than can be obtained by Hiramatsu and Oka equations, here we carry out a parametric finite-element study of the test, in which an isotropic elastic sphere is diametrically compressed by isotropic elasto-plastic platens. By performing a large number of finite element simulations under a range of conditions, we propose a set of simple expressions that can replace the Hiramatsu and Oka equations and be used to quickly, yet accurately (to within $\approx 5\%$), estimate the hoop strength of compressed spherical particles.

The problem is of course far from new: the mechanics of the embedding of various objects, e.g. spheres, discs or cylinders, as they are pushed against a flat deformable surface, has been studied both analytically and numerically in many settings, for example due to its connection with the Brinell hardness tests or instrumented indentation tests used to assess various material mechanical properties (Hill et al., 1989; Bower et al., 1993; Biwa and Storkers, 1995; Huber and Tsakmakis, 1998; Mesarovic and Fleck, 1999; Kucharski and Mrz, 2001; Sakai et al., 2003; Kogut and Komvopoulos, 2004; Niederkofler et al., 2009; Ghaednia et al., 2016; Clausner and Richter, 2016). In these studies, it is shown that the indentation laws, i.e., the dependence of the indentation load on the indentation depth (or equivalently on the contact radius), depend strongly on the elasto-plastic parameters of the indented material. Contact friction stresses mainly affect the indented material stress distribution while being less important for the indentation response itself (Bower et al., 1993; Mesarovic and Fleck, 1999). Often, the indenting object is assumed to be rigid; however, there are finite element analyses in which a deformable (elastic or elasto-plastic) sphere is compressed by a rigid flat surface. Such studies have been conducted in the context of contact mechanics (Kogut and Etsion, 2002; Jackson and Green, 2005; Malayalamurthi and Marappan, 2008) or to understand the mechanics and fracture of elastic or elasto-plastic discs and cylinders that are diametrically compressed between two rigid platens, to model the Brazilian disc test or the compressive point–load test (Procopio et al., 2003; Es-Saheb et al., 2011). None of those studies, however, answer the question posed here, namely what could cause a brittle sphere to fail when compressed between two deformable platens: in work to date spheres are considered to be rigid, the investigations are limited to small contact radii a/R, or discs and cylinders are considered instead of a sphere. We thus examine here in detail, with a goal to complement analytical studies such as that of Hiramatsu and Oka, the evolution of stress within an elastic sphere that is diametrically compressed between two elasto-plastic platens up to large contact radii, with focus on (tensile) stresses within the sphere that might cause it to fracture.

2. Methods: the finite element model

Finite element modeling of an isotropic elastic sphere of radius R subjected to a diametric compression by a pair of elasto–plastic platens was implemented in Abaqus FEA v6.11 (Dassault Systèmes Simulia Corp., Providence, RI, USA) software as a Python script, which is made freely available on the website of our laboratory (http://lmm.epfl.ch). These models can be used to extract other output than parameters discussed here (e.g., stress and strain values at other locations in the sphere than the center or the equator). Note that in this case the convergence of results need to be rechecked directly with respect to the other output parameter. Here used models were specifically optimized to yield converged results mainly for the stress values in the center and at the equator of the sphere.

Due to symmetry of the problem, only one-half of the axisymmetric model need be considered (Fig. 1).

Linear isotropic elastic behaviour of the sphere and the platen is described via their Young's moduli and Poisson's ratios, E_s, ν_s and E_p, ν_p, respectively. The platen plastic behaviour is modeled using isotropic J_2 flow theory and the three-parameter exponential hardening law, $\sigma_{vM} = Y_0 + Y_1 \varepsilon_p^m$, where σ_{vM} is the von Mises stress, ε_p is the equivalent plastic strain and Y_0, Y_1 and m are the platen material parameters for the yield strength, the rate of hardening and the hardening exponent, respectively. Contact friction between the sphere and the platens is explicitly included in the model – hard contact for the normal direction, and Coulomb friction with a constant friction coefficient μ for the tangential direction along the sphere–platen contact surface.

The size of the rectangular platen domain and the mesh were both optimized in preliminary (convergence) runs in order to determine the domain size beyond which there is no influence on the magnitude of the

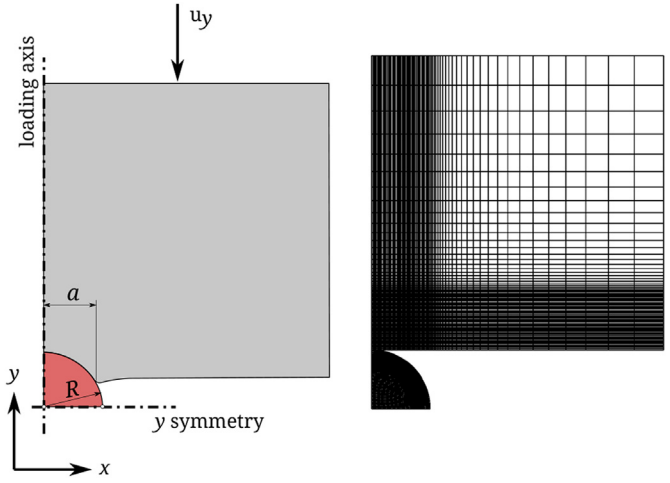

Fig. 1. An axisymmetric finite element model of a diametrically compressed sphere.

first principal stress in the center of the sphere or along the sphere equator. This led to fix the platen domain size used for production calculations at $5R$. The sphere domain as well as the platen domain in contact with the sphere are meshed with a finer mesh and element size $R/50$. Outside the contact zone, the platen domain is gradually coarsened. Both the sphere and the platen domains are discretized using quadratic (CAX8) quadrilateral elements. Loading in the model is applied by prescribing the total vertical displacement u_y along the top edge of the platen part. Simulations were run with automatic displacement increment stepping control. All calculations account for nonlinear geometrical effects. Typically, each simulation required about one to a few hundred displacement increments, during which the sphere was gradually embedded up to a relative contact radius $\approx 0.9a/R$.

During each simulation several quantities were extracted for each displacement increment step. The first principal stress at the sphere center or on the equator, σ_{1C} and σ_{1E}, respectively, were recorded as standard Abaqus output. The total load applied was obtained by integrating the vertical components of the nodal reaction forces along the platen top edge. The contact radius a was extracted as the x-coordinate of the point along the sphere surface at which the contact pressure p dropped to zero.

3. Results and discussion

Hiramatsu and Oka (HO) reduced the sphere compression problem to a boundary value problem, where the constant applied pressure p and the contact radius a are independently prescribed boundary conditions. Their solution established the functional dependence, $\tilde{\sigma}_1(r, \theta, \phi) = f(a/R, \nu_s, r, \theta, \phi)$, between the following dimensionless parameters: (i) the normalized first (tensile) principal stress, $\tilde{\sigma}_1 = \sigma_1 \pi R^2/F$, at a point (r, θ, ϕ) of the sphere, (ii) the relative contact radius, a/R, and (iii) the sphere Poisson's ratio, ν_s. The total load F used to normalize the principal stress σ_1 in the HO equations is the integrated pressure p that acts over the area of the two spherical caps defined by a/R, i.e, $F = p \times 2\pi R^2\{1 - \cos[\arcsin(a/R)]\}$. Now, when an elastic sphere is compressed by the elasto–plastic platens under increasing compressive load F, the sphere is gradually pushed into the platens, the relative contact radius a/R increases, the stress field within the sphere also evolves and, importantly, the contact stress conditions also change. For small a/R, both the sphere and the platens deform elastically. The contact stress is then expected to be purely normal, as established in Hertzian contact theory (Johnson, 2003; Chen et al., 2006); the sphere compression problem of Hiramatsu and Oka adapted for the Hertz pressure was addressed by Chau et al. (2000). At higher a/R, the contact stress becomes more complicated since, in addition to the normal pressure, friction along the area of contact is expected to give rise to a nonuniform tangential stress component, which increases with the distance from the loading axis and reaches a maximum somewhere near the contact end, as was observed for the case when an elasto-plastic flat surface is indented by a rigid sphere and the contact law is one of perfect sticking (Bower et al., 1993).

To investigate the stress field of a sphere during diametric compression by elasto–plastic platens, we extend the HO parameter space to include dimensionless parameters that govern the behaviour of elasto-plastic platens and the contact surface. Because of its importance for the interpretation of the diametric compression strength tests of spheres at larger relative contact areas, we discuss results with focus on first principal stress values at two points of the sphere, shown by the HO analysis (and confirmed by present results) to be the two locations at which the most elevated tensile stress is found in the sphere, namely: (i) the sphere center, where the first principal stress is σ_{1C} and (ii) the sphere equator with hoop stress σ_{1E}. Preliminary FE calculations (see Fig. S1, Supplementary Information) were carried out to probe the influence of the Poisson's ratio of the platen material ν_p; varying only this parameter in the range from 0.1 to 0.4 while keeping all other parameters fixed had a negligible influence on the sphere principal (tensile) stresses $\tilde{\sigma}_{1C}$ and $\tilde{\sigma}_{1E}$. Thus, in the following, this parameter was fixed at $\nu_p = 0.3$ in all simulations. The dependence of the sphere's normalized first principal stress on remaining system parameters, i.e.

$$\tilde{\sigma}_1 = f\left(\frac{a}{R}, \nu_s, \frac{E_s}{E_p}, \frac{E_p}{Y_0}, \frac{Y_0}{Y_1}, m, \mu\right), \tag{1}$$

is then investigated as follows.

For the parametric study we consider combinations of different parameters that span a large space of hypothetical but realistic sphere and platen materials. The simulations were thus conducted for values of the Young's modulus and the Poisson's ratio of the sphere, $E_s \in (100{,}400)$ GPa and $\nu_s \in (0.15, 0.20, 0.25, 0.30, 0.35, 0.40)$, respectively. For platens, we choose a Young's modulus $E_p = 200$ GPa (near that of steel, the most likely material used in the present approach), yield strengths, $Y_0 \in (0.6, 1.5)$ GPa, hardening strengths, $Y_1 \in (0, Y_0)$ GPa, and hardening exponents, $m \in (0.3, 0.5)$. Considered sphere–platen friction coefficients are $\mu \in (0{,}0.1, 0.2, 0.3)$. This combination of model parameters resulted in dimensionless parameter variations such that the ratio E_s/E_p was effectively varied from 0.5 to 2, the ratio E_p/Y_0 was equal to 333 or 133, while for the platen plastic behaviour we considered the perfectly-plastic case ($Y_1 = 0$) and two realistic strain hardening behaviours (namely $Y_1/Y_0 = 1$ and $m = 0.3, 0.5$) all with different yield strength values. In total we carried out 72 different simulations for each friction coefficient, thus 4×72 simulations in total.

Fig. 2a and b show superimposed evolutions of the sphere's normalized principal stresses, $\tilde{\sigma}_{1C}$ and $\tilde{\sigma}_{1E}$, versus a/R, as obtained from 72 different FE simulations, all with friction coefficient $\mu = 0.1$.

From Fig. 2a and b it is clear that the Poisson's ratio of the sphere, ν_s, is a parameter that strongly affects the sphere's stress field at any a/R, a fact that was already shown by the HO equations. Increasing ν_s generally increases $\tilde{\sigma}_{1E}$ and decreases $\tilde{\sigma}_{1C}$ at any a/R.

The effect that the parameters E_s/E_p, E_p/Y_0, and m have on the stresses $\tilde{\sigma}_{1C}$ and $\tilde{\sigma}_{1E}$ seems to be of much less importance over a wide range of a/R values, since the results of simulations for different E_s/E_p, E_p/Y_0, and m but constant ν_s are all grouped near one another. At small a/R, the Young's modulus mismatch between the sphere and the platens as well as the platen plastic behaviour do not affect significantly the stress at the center of the sphere $\tilde{\sigma}_{1C}$ or along the equator $\tilde{\sigma}_{1E}$. The two points of interest seem to be sufficiently far from the location of load application for the specifics of how stress is distributed along the sphere surface to have little importance (as expected from the Saint-Venant principle). At higher a/R, variations in parameters E_s/E_p, E_p/Y_0, and m introduce small variations in $\tilde{\sigma}_{1C}$ and $\tilde{\sigma}_{1E}$. The most important parameter

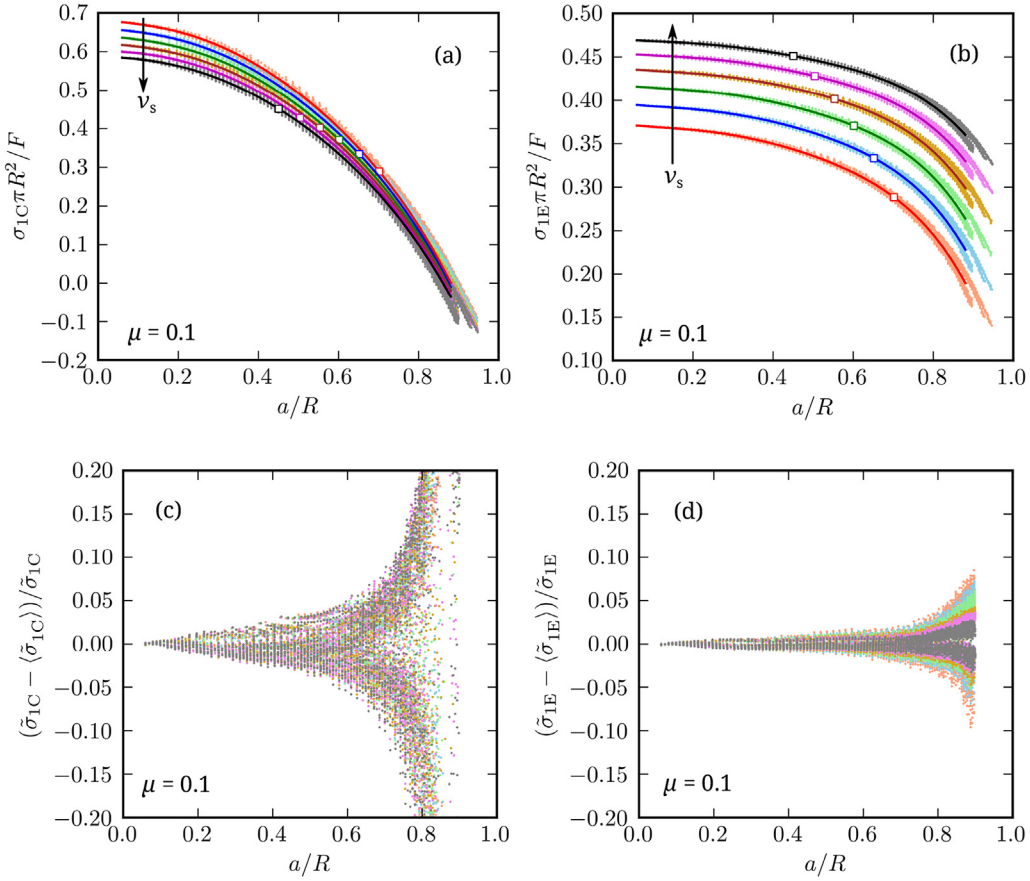

Fig. 2. Normalized first principal stress (a) in the center of the sphere, $\tilde{\sigma}_{1C}$, and (b) along the equator, $\tilde{\sigma}_{1E}$, versus a/R. Light colour indicates data obtained for 72 different FE simulations all with friction coefficient $\mu = 0.1$. The lines are least-square fits, $\hat{\tilde{\sigma}}_{1C}$ and $\hat{\tilde{\sigma}}_{1E}$, to all FE data for $\tilde{\sigma}_{1C}$ and $\tilde{\sigma}_{1E}$, respectively, at constant ν_s and for a/R values in the range from 0.05 to 0.9. The Poisson's ratios of the sphere in the direction of the arrow are: 0.15, 0.20, 0.25, 0.30, 0.35 and 0.40. The square symbols for each ν_s represents the a/R value above which $\tilde{\sigma}_{1E} > \tilde{\sigma}_{1C}$. Relative errors of the fits to the FE data from panels (a) and (b) are shown in (c) for the sphere center, and (d) for the sphere equator. (For interpretation of the references to colour in this figure legend, the reader is referred to the Web version of this article.)

of these three is the platen hardening exponent m; for increasing m both $\tilde{\sigma}_{1C}$ and $\tilde{\sigma}_{1E}$ decrease a bit at high a/R (see Fig. S2, Supplemental Information).

Because the effect that elasto-plastic platen parameters have on the sphere stresses $\tilde{\sigma}_{1C}$ and $\tilde{\sigma}_{1E}$ is small and complex, we do not investigate in depth nor do we develop full scaling laws for the sphere stress $\tilde{\sigma}_{1C}$ and $\tilde{\sigma}_{1E}$ here. Instead, we view these variations simply as sources of scatter around the mean stress values, e.g. $\langle\tilde{\sigma}_{1C}\rangle$ and $\langle\tilde{\sigma}_{1E}\rangle$, found in the present set of simulations. If all the different FE results for $\tilde{\sigma}_{1C}$ and $\tilde{\sigma}_{1E}$ at constant ν_s, shown in Fig. 2a and b, are considered together and fitted by a polynomial function to obtain the approximations $\langle\tilde{\sigma}_{1C}\rangle$ and $\langle\tilde{\sigma}_{1E}\rangle$ for the stresses $\tilde{\sigma}_{1C}$ and $\tilde{\sigma}_{1E}$ in the mean sense, respectively, then the relative errors between the fits, $\langle\tilde{\sigma}_{1C}\rangle$ and $\langle\tilde{\sigma}_{1E}\rangle$, and the individual data points for $\tilde{\sigma}_{1C}$ and $\tilde{\sigma}_{1E}$, are indeed small over the large range of contact radii a/R explored here, as shown in Fig. 2c and d. Relative error values that exceed $\approx$ 5% for $\tilde{\sigma}_{1E}$ are found only for a/R greater than ≈ 0.85 (Fig. 2d), while for $a/R \approx 0.9$ the error, at $\approx$ 7%, remains still acceptably small. For $\tilde{\sigma}_{1C}$, the relative errors exceed $\approx$ 5% above $a/R \approx 0.6$ (Fig. 2c). Note however, that near $a/R \approx 0.6$ and somewhat depending on ν_s, the stress on the equator $\tilde{\sigma}_{1E}$ is equal to or greater than the stress in the center $\tilde{\sigma}_{1C}$ of the sphere (as is indicated by the square in Fig. 2a and b). The fact that the relative error in $\tilde{\sigma}_{1C}$ increases strongly beyond $a/R \approx 0.6$ is therefore of relatively minor significance when evaluating the surface strength of a sphere, since it is the hoop stress $\tilde{\sigma}_{1E}$ that is important at such high a/R: this quantity is still accurately approximated by $\langle\tilde{\sigma}_{1E}\rangle$ all the way up to $a/R \approx 0.9$ for a wide range of sphere and platen materials.

A similar series of calculations and analyses as was performed for $\mu = 0.1$ in Fig. 2, was performed with other friction coefficients. Results of sets of FE simulations obtained for friction coefficients $\mu = 0$, 0.2 and 0.3 are given in the Supplemental Information, in Figs. S3, S4 and S5, respectively. Observations made above for the case $\mu = 0.1$ are found to be equally applicable for other friction coefficients explored here (see Figs. S3, S4 and S5). Generally, variations of $\tilde{\sigma}_{1C}$ and $\tilde{\sigma}_{1E}$ that are introduced via variations of the parameters E_s/E_p, E_p/Y_0, and m remain reasonably small for any data set with constant ν_s and μ. As a consequence, the fitted polynomial approximations, $\langle\tilde{\sigma}_{1C}\rangle$ and $\langle\tilde{\sigma}_{1E}\rangle$, to those data sets remain rather accurate, yet very simple, descriptors for the sphere stresses $\tilde{\sigma}_{1C}$ and $\tilde{\sigma}_{1E}$ over a wide range of contact radii a/R.

Because of its direct importance for the evaluation of sphere strength in diametrically compressed sphere testing at large a/R, the coefficients $c_i(\nu_s, \mu)$ and $e_i(\nu_s, \mu)$ that are valid for polynomial expansions of the present results up to 5th order and a/R in the range from 0.05 to 0.9 for $\langle\tilde{\sigma}_{1C}\rangle$ and $\langle\tilde{\sigma}_{1E}\rangle$, i.e.

$$\langle\tilde{\sigma}_{1C}(a/R, \nu_s, \mu)\rangle = \sum_{i=0}^{5} c_i(\nu_s, \mu)(a/R)^i, \tag{2}$$

$$\langle\tilde{\sigma}_{1E}(a/R, \nu_s, \mu)\rangle = \sum_{i=0}^{5} e_i(\nu_s, \mu)(a/R)^i, \tag{3}$$

are tabulated for different ν_s and μ values in Table 1 and Table 2, respectively.

In Fig. 3a and b, the normalized sphere stresses, $\tilde{\sigma}_{1C}$ and $\tilde{\sigma}_{1E}$, obtained from the HO equations (dotted lines) are confronted with the present numerical solutions, $\langle\tilde{\sigma}_{1C}\rangle$ and $\langle\tilde{\sigma}_{1E}\rangle$, obtained via Eqs. (2) and (3) with coefficients, c_i and e_i taken from Tables 1 and 2 for various

Table 1
Coefficients, $c_i(\nu_s, \mu)$, of polynomial expansion given by Eq. (2), for different sphere Poisson's ratios ν_s and sphere/platen friction coefficients μ. Coefficients are valid for a/R in the range from 0.05 to 0.9.

c_0	c_1	c_2	c_3	c_4	c_5	ν_s	μ
0.6800	−0.0547	0.1094	−2.6329	3.4841	−1.8932	0.15	0.0
0.6577	−0.0272	−0.0695	−2.0839	2.7790	−1.5591	0.20	0.0
0.6408	−0.0828	0.2750	−2.9792	3.8546	−2.0292	0.25	0.0
0.6196	−0.0248	−0.0975	−1.9402	2.6360	−1.5119	0.30	0.0
0.6031	−0.0353	−0.0519	−1.9426	2.4991	−1.3841	0.35	0.0
0.5871	−0.0314	−0.0521	−2.0271	2.7590	−1.5647	0.40	0.0
0.6834	−0.1289	0.3472	−3.3132	4.3167	−2.2143	0.15	0.1
0.6617	−0.1095	0.2277	−2.9247	3.8462	−2.0172	0.20	0.1
0.6436	−0.1385	0.4314	−3.4271	4.4048	−2.2356	0.25	0.1
0.6221	−0.0711	−0.0250	−2.0480	2.6426	−1.4227	0.30	0.1
0.6025	−0.0191	−0.3413	−1.1733	1.6149	−0.9857	0.35	0.1
0.5876	−0.0358	−0.1945	−1.6477	2.2959	−1.3164	0.40	0.1
0.6803	−0.0456	−0.3316	−1.4813	2.0139	−1.1122	0.15	0.2
0.6615	−0.0937	0.0441	−2.5250	3.3266	−1.7072	0.20	0.2
0.6373	0.0026	−0.5259	−0.9657	1.4715	−0.9035	0.25	0.2
0.6181	0.0211	−0.6712	−0.3756	0.5870	−0.4459	0.30	0.2
0.6019	0.0001	−0.4518	−1.0621	1.5065	−0.8694	0.35	0.2
0.5839	0.0482	−0.7558	−0.2333	0.5723	−0.4881	0.40	0.2
0.6799	−0.0477	−0.2625	−1.7409	2.2356	−1.1379	0.15	0.3
0.6540	0.0619	−0.9485	0.1874	−0.0848	−0.1210	0.20	0.3
0.6335	0.0837	−1.0572	0.4985	−0.4363	0.0360	0.25	0.3
0.6152	0.0681	−0.7836	−0.4976	0.9579	−0.6131	0.30	0.3
0.6035	−0.0264	−0.2807	−1.4480	1.7219	−0.8147	0.35	0.3
0.5850	0.0366	−0.6430	−0.5792	0.8651	−0.5109	0.40	0.3

Table 2
Coefficients, $e_i(\nu_s, \mu)$, of polynomial expansion given in Eq. (3), for different sphere Poisson's ratios ν_s and sphere/platen friction coefficients μ. Coefficients are valid for a/R in the range from 0.05 to 0.9.

e_0	e_1	e_2	e_3	e_4	e_5	ν_s	μ
0.3736	−0.0648	0.4338	−1.6901	2.3097	−1.2911	0.15	0.0
0.3970	−0.0607	0.4147	−1.5828	2.1582	−1.2013	0.20	0.0
0.4189	−0.0703	0.4893	−1.7575	2.3760	−1.2857	0.25	0.0
0.4377	−0.0570	0.4091	−1.4876	2.0184	−1.0978	0.30	0.0
0.4548	−0.0446	0.3281	−1.2002	1.6223	−0.8889	0.35	0.0
0.4707	−0.0387	0.3003	−1.0958	1.4846	−0.8071	0.40	0.0
0.3745	−0.0830	0.4782	−1.8574	2.5612	−1.4250	0.15	0.1
0.3979	−0.0777	0.4399	−1.7073	2.3753	−1.3322	0.20	0.1
0.4196	−0.0813	0.4696	−1.7701	2.4646	−1.3636	0.25	0.1
0.4381	−0.0600	0.3218	−1.2929	1.8287	−1.0441	0.30	0.1
0.4555	−0.0546	0.2996	−1.2213	1.7464	−0.9938	0.35	0.1
0.4711	−0.0414	0.2257	−1.0077	1.4839	−0.8575	0.40	0.1
0.3731	−0.0509	0.2503	−1.3003	1.9021	−1.1326	0.15	0.2
0.3978	−0.0738	0.4156	−1.7643	2.5008	−1.3980	0.20	0.2
0.4176	−0.0397	0.1963	−1.1248	1.6939	−1.0136	0.25	0.2
0.4381	−0.0581	0.3095	−1.3766	1.9483	−1.0918	0.30	0.2
0.4557	−0.0586	0.3361	−1.4580	2.0484	−1.1156	0.35	0.2
0.4711	−0.0415	0.2409	−1.2039	1.7513	−0.9724	0.40	0.2
0.3733	−0.0595	0.3211	−1.4984	2.0780	−1.1789	0.15	0.3
0.3953	−0.0217	0.0707	−0.7677	1.1633	−0.7525	0.20	0.3
0.4169	−0.0247	0.0925	−0.7987	1.1738	−0.7296	0.25	0.3
0.4369	−0.0375	0.2230	−1.2105	1.7040	−0.9528	0.30	0.3
0.4562	−0.0663	0.3959	−1.5834	2.0470	−1.0493	0.35	0.3
0.4717	−0.0503	0.3198	−1.4241	1.9136	−1.0004	0.40	0.3

values of ν_s and friction coefficients $\mu = 0$ (dashed lines) or $\mu = 0.3$ (solid lines).

As can be seen in Fig. 3, the HO solution agrees with our numerical results only for small a/R, roughly up to $a/R \leq 0.2$. As argued above, for small a/R, the specific stress distribution under which the sphere is loaded has limited relevance on the stress at remote locations within the sphere, at its center or along the equator, such that an assumption of a uniformly applied contact pressure p is as good as nearly any other assumption of this kind. At higher a/R however, both normal and tangential contact stresses and the greater size of the loading surface in relation to the sphere cross section begin to influence the sphere's stress field everywhere, thereby causing the HO predictions to significantly deviate from the more accurate stress predictions obtained by means of FE simulations. The effect of the contact friction μ on $\tilde{\sigma}_{1C}$ and $\tilde{\sigma}_{1E}$ is such that, increasing μ, generally causes both $\tilde{\sigma}_{1C}$ and $\tilde{\sigma}_{1E}$ to decrease all else constant, as intuition would suggest. This decrease is more pronounced for the hoop stress $\tilde{\sigma}_{1E}$ (Fig. 3b) than for the stress in the sphere's center $\tilde{\sigma}_{1C}$ (Fig. 3a).

In Tables 1 and 2 the coefficients, c_i and e_i, in Eqs. (2) and (3) are tabulated for discrete values of parameters ν_s and μ. Approximate values for coefficients at intermediate values of ν_s and μ can be obtained by simple bilinear interpolation:

$$\sigma(\nu_s, \mu) \approx \frac{1}{A}\mathbf{v}_\nu^{\mathrm{T}}\begin{bmatrix}\sigma(\nu_{s1}, \mu_1) & \sigma(\nu_{s1}, \mu_2)\\ \sigma(\nu_{s2}, \mu_1) & \sigma(\nu_{s2}, \mu_2)\end{bmatrix}\mathbf{v}_\mu, \tag{4}$$

with the vectors,

$$\mathbf{v}_\nu^{\mathrm{T}} = [\nu_{s2} - \nu_s, \nu_s - \nu_{s1}],$$
$$\mathbf{v}_\mu = [\mu_2 - \mu, \mu - \mu_1]^{\mathrm{T}}, \tag{5}$$

and the constant $A = (\nu_{s2} - \nu_{s1})(\mu_2 - \mu_1)$, where σ is either $\langle\tilde{\sigma}_{1C}\rangle$ or $\langle\tilde{\sigma}_{1E}\rangle$, respectively, and ν_{s1}, ν_{s2} and μ_1, μ_2 are known parameters from Tables 1 and 2 that bound the intermediates ν_s and μ, respectively, i.e. $\nu_{s1} < \nu_s < \nu_{s2}$ and $\mu_1 < \mu < \mu_2$. By using bilinear interpolation to predict the intermediate cases of $\nu_s = 0.2$, 0.25, 0.3 or 0.35 at constant μ from solutions for $\nu_{s1} = 0.1$ and $\nu_{s2} = 0.4$, the relative error of predictions with respect to the known solutions given in Tables 1 and 2 is found to be of only a few percent (up to $\approx 5\%$). Similarly small relative errors of no more than $\approx 5\%$ are found if cases for $\mu = 0.1$ and 0.2 at constant ν_s are interpolated form the solutions for $\mu_1 = 0$ and $\mu_2 = 0.3$. Thus, it can reasonably be expected that the bilinear interpolation of other intermediate cases will give similarly small relative error.

4. Conclusion

Using the finite element method, we study here the problem of an elastic sphere that is diametrically compressed between two flat parallel elasto-plastic platens assuming hard contact behaviour normal to the contact surface and Coulomb friction for the tangential contact behaviour. A parametric study is conducted considering a wide range of realistic sphere and platen material parameters and friction coefficients. It is shown that the normalized first principal stress in the center of the sphere, $\tilde{\sigma}_{1C}$, and the hoop stress along the sphere's equator, $\tilde{\sigma}_{1E}$, which depend strongly on the contact radius a/R and the Poisson's ratio ν_s, are also affected by the friction coefficient μ. On the other hand, the dependence of $\tilde{\sigma}_{1C}$ and $\tilde{\sigma}_{1E}$ on the elasto-plastic parameters or Poisson ratio of the platen material is found to be weak. As a result, simple yet relatively accurate expressions can be proposed to quickly estimate the stresses $\tilde{\sigma}_{1C}$ and $\tilde{\sigma}_{1E}$ for various ν_s and μ.

It is found that the Hiramatsu and Oka equations are applicable to the diametric compression of spheres only for small contact radii, roughly up to $a/R \leq 0.2$. Beyond this contact radius, the Hiramatsu and Oka equations start to increasingly underestimate the sphere stresses, $\tilde{\sigma}_{1C}$ and $\tilde{\sigma}_{1E}$, and cannot account for the dependence of those parameters on sphere–platen contact behaviour.

Turning to practical aspects of spherical particle compression testing for strength, the fact that normalized (peak tensile) first principal stresses, $\tilde{\sigma}_{1C}$ and $\tilde{\sigma}_{1E}$, depend little on the platen elasto-plastic behaviour, brings a significant simplification in data interpretation. Since the platen behaviour will govern the sphere indentation process and establish the indentation law linking the applied indentation load F and the contact radius a/R, to compute the physical stress values (in units of Pa) from the dimensionless quantities $\tilde{\sigma}_{1C}$ and $\tilde{\sigma}_{1E}$, knowledge of the indentation law is nonetheless needed; however, since the information obtained from the diametric compression tests should at least include a measurement of the load at failure, e.g. F_c and the corresponding critical contact radius, e.g. a_c/R , the indentation law that

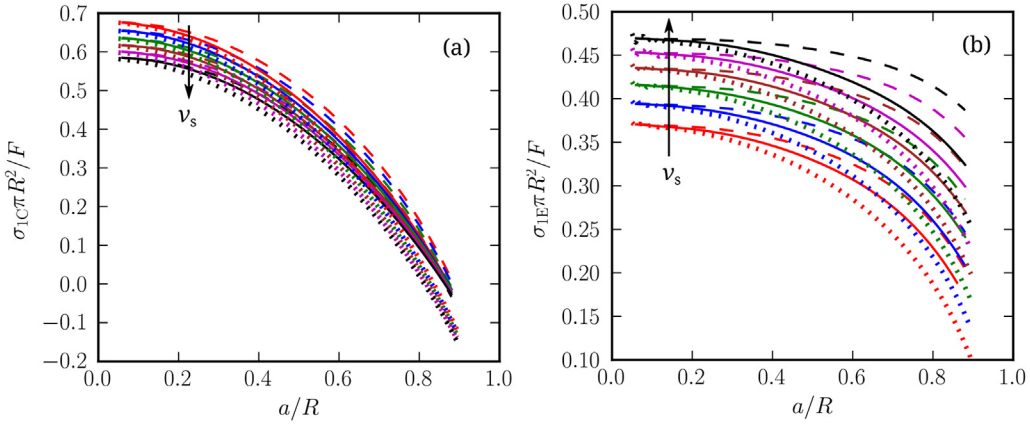

Fig. 3. Comparison of the solutions for (a) $\widetilde{\sigma}_{1C}$, and (b) $\widetilde{\sigma}_{1E}$ as obtained from the HO equations (dotted lines) and by Eqs. (2) and (3), respectively, for Poisson's ratio in the direction of the arrow $\nu_s = 0.15$, 0.2, 0.25, 0.3, 0.35 and 0.4, and for friction coefficients $\mu = 0$ (dashed lines) and 0.3 (solid lines).

governs the particle sinking into the platens can be directly recreated from these experimental data, either by using numerically established scaling relations (Hill et al., 1989; Mesarovic and Fleck, 1999) or empirical relations such as Meyer's law (Pejchal et al., 2017, 2018).

As a final remark, it is worth emphasizing that the results obtained here were obtained by assuming that the compressed sphere behaves as a linear elastic and brittle material. The material behaviour of a compressed real particle, however, can deviate therefrom as a result of the high stress values that may be reached, and may do so for various reasons, such as higher-order (non-linear) elasticity, plasticity caused by dislocation nucleation and motion, pressure-induced phase transformation, twinning or densification.

Acknowledgments

This work was supported by the European Research Council under the European Union's Seventh Framework Programme (FP/2007–2013)/ ERC Advanced Grant Agreement No. 291085.

Appendix A. Supplementary data

Supplementary data related to this article can be found at http://dx.doi.org/10.1016/j.euromechsol.2018.04.016.

References

Aman, S., Tomas, J., Kalman, H., 2010. Breakage probability of irregularly shaped particles. Chem. Eng. Sci. 65 (5), 1503–1512.
Antonyuk, S., Tomas, J., Heinrich, S., Mrl, L., 2005. Breakage behaviour of spherical granulates by compression. Chem. Eng. Sci. 60 (14), 4031–4044.
Biwa, S., Storkers, B., 1995. An analysis of fully plastic Brinell indentation. J. Mech. Phys. Solid. 43 (8), 1303–1333.
Bower, A.F., Fleck, N.A., Needleman, A., Ogbonna, N., 1993. Indentation of a power law creeping solid. Proc. R. Soc. London A: Math. Phys. Eng. Sci. 441 (1911), 97–124.
Chau, K.T., Wei, X.X., 1999. Spherically isotropic, elastic spheres subject to diametral point load strength test. Int. J. Solid Struct. 36 (29), 4473–4496.
Chau, K.T., Wei, X.X., Wong, R.H.C., Yu, T.X., 2000. Fragmentation of brittle spheres under static and dynamic compressions: experiments and analyses. Mech. Mater. 32 (9), 543–554.
Chen, Y., Best, A., Butt, H.-J., Boehler, R., Haschke, T., Wiechert, W., 2006. Pressure distribution in a mechanical microcontact. Appl. Phys. Lett. 88 (23), 234101.
Chen, Y., Best, A., Haschke, T., Wiechert, W., Butt, H.-J., 2007. Stress and failure at mechanical contacts of microspheres under uniaxial compression. J. Appl. Phys. 101 (8), 084908.
Clausner, A., Richter, F., 2016. Fundamental Limitations at the Determination of Initial Yield Stress Using Nano-indentation with Spherical Tips, vol. 58. pp. 69–75.
Darvell, B.W., 1990. Uniaxial compression tests and the validity of indirect tensile strength. J. Mater. Sci. 25 (2), 757–780.
Dean, B.W., Sneddon, I.M., Parsons, H.W., 1952. Distribution of stress in decelerating elastic sphere. In: Selected Government Research Reports: Strength and Testing of Materials: Part II: Testing Methods and Test Results. HMSO, London.
Es-Saheb, M.H., Albedah, A., Benyahia, F., 2011. Diametral compression test: validation using finite element analysis. Int. J. Adv. Manuf. Technol. 57 (5–8), 501–509.
Gerberich, W.W., Mook, W., Perrey, C., Carter, C., Baskes, M., Mukherjee, R., Gidwani, A., Heberlein, J., McMurry, P., Girshick, S., 2003. Superhard silicon nanospheres. J. Mech. Phys. Solid. 51 (6), 979–992.
Ghaednia, H., Pope, S.A., Jackson, R.L., Marghitu, D.B., 2016. A comprehensive study of the elasto-plastic contact of a sphere and a flat. Tribol. Int. 93 (Part A), 78–90.
Hill, R., Storakers, B., Zdunek, A.B., 1989. A theoretical study of the Brinell hardness test. Proc. R. Soc. London A: Math. Phys. Eng. Sci. 423 (1865), 301–330.
Hiramatsu, Y., Oka, Y., 1966. Determination of the tensile strength of rock by a compression test of an irregular test piece. Int. J. Rock Mech. Min. Sci. 3, 89–99.
Hiramatsu, Y., Oka, Y., 1967. Determination of the tensile strength of rock by a compression test of an irregular test piece. Int. J. Rock Mech. Min. Sci. Geomech. Abstr. 4 (3), 363–365.
http://lmm.epfl.ch.
Huang, J., Xu, S., Yi, H., Hu, S., 2014. Size effect on the compression breakage strengths of glass particles. Powder Technol. 268, 86–94.
Huber, N., Tsakmakis, C., 1998. A finite element analysis of the effect of hardening rules on the indentation test. J. Eng. Mater. Technol. 120 (2), 143–148.
Jackson, R.L., Green, I., 2005. A finite element study of elasto-plastic hemispherical contact against a rigid flat. J. Tribol. 127 (2), 343–354.
Jaeger, J.C., 1967. Failure of rocks under tensile conditions. Int. J. Rock Mech. Min. Sci. Geomech. Abstr. 4 (2), 219–227.
Johnson, K.L., 2003. Contact Mechanics. Cambridge University Press.
Khanal, M., Schubert, W., Tomas, J., 2005. DEM simulation of diametrical compression test on particle compounds. Granul. Matter 7 (2–3), 83–90.
Kogut, L., Etsion, I., 2002. Elastic-plastic contact analysis of a sphere and a rigid flat. J. Appl. Mech. 69 (5), 657–662.
Kogut, L., Komvopoulos, K., 2004. Analysis of the spherical indentation cycle for elasticperfectly plastic solids. J. Mater. Res. 19 (12), 3641–3653.
Kucharski, S., Mrz, Z., 2001. Identification of plastic hardening parameters of metals from spherical indentation tests. Mater. Sci. Eng., A 318 (12), 65–76.
Malayalamurthi, R., Marappan, R., 2008. Elastic-plastic contact behavior of a sphere loaded against a rigid flat. Mech. Adv. Mater. Struct. 15 (5), 364–370.
Mazel, V., Guerard, S., Croquelois, B., Kopp, J.B., Girardot, J., Diarra, H., Busignies, V., Tchoreloff, P., 2016. Reevaluation of the diametral compression test for tablets using the flattened disc geometry. Int. J. Pharm. 513 (12), 669–677.
Mcdowell, G.R., Amon, A., 2000. The application of weibull statistics to the fracture of soil particles. Soils Found. 40 (5), 133–141.
McDowell, G.R., Bolton, M.D., 1998. On the micromechanics of crushable aggregates. Gotechnique 48 (5), 667–679.
Mesarovic, S.D., Fleck, N.A., 1999. Spherical indentation of elastic-plastic solids. Proc. Math. Phys. Eng. Sci. 455 (1987), 2707–2728.
Mook, W., Nowak, J., Perrey, C., Carter, C., Mukherjee, R., Girshick, S., McMurry, P., Gerberich, W., 2007. Compressive stress effects on nanoparticle modulus and fracture. Phys. Rev. B 75 (21), 1–10.
Niederkofler, T., Jger, A., Lackner, R., 2009. Identification of model parameters from elastic/elasto-plastic spherical indentation. Int. J. Mater. Res. 100 (7), 926–932.
Ogiso, H., Yoshida, M., Nakano, S., Akedo, J., 2007. Effects of Al ion implantation on the strength of Al2o3 particles. Surf. Coating. Technol. 201 (19–20), 8180–8184.
Pejchal, V., Žagar, G., Charvet, R., Dénéréaz, C., Mortensen, A., 2017. Compression testing spherical particles for strength: theory of the meridian crack test and implementation for microscopic fused quartz. J. Mech. Phys. Solid. 99, 70–92.
Pejchal, V., Fornabaio, M., Žagar, G., Riesen, G., Romain, M., Medřický, G., Chráska, T., Mortensen, A., 2018. The strength of plasma–sprayed amorphous and nanocrystalline ceramic microparticles measured by means of the meridian crack test. Acta Mater. 145, 278–289.
Pitchumani, R., Zhupanska, O., Meesters, G.M.H., Scarlett, B., 2004. Measurement and characterization of particle strength using a new robotic compression tester. Powder Technol. 143144, 56–64.
Portnikov, D., Kalman, H., Aman, S., Tomas, J., 2013. Investigating the testing procedure limits for measuring particle strength distribution. Powder Technol. 237, 489–496.
Procopio, A.T., Zavaliangos, A., Cunningham, J.C., 2003. Analysis of the diametrical

compression test and the applicability to plastically deforming materials. J. Mater. Sci. 38 (17), 3629–3639.
Ribas, L., Cordeiro, G.C., Toledo Filho, R.D., Tavares, L.M., 2014. Measuring the strength of irregularly-shaped fine particles in a microcompression tester. Miner. Eng. 65, 149–155.
Rozenblat, Y., Portnikov, D., Levy, A., Kalman, H., Aman, S., Tomas, J., 2011. Strength distribution of particles under compression. Powder Technol. 208 (1), 215–224.
Sakai, M., Akatsu, T., Numata, S., Matsuda, K., 2003. Linear strain hardening in elasto-plastic indentation contact. J. Mater. Res. 18 (9), 2087–2096.
Salençon, J., 1966. Comments on determination of the tensile strength of rock by a compression test of an irregular test piece. Int. J. Rock Mech. Min. Sci. Geomech. Abstr. 3 (4), 349–350.
Schönert, K., 2004. Breakage of spheres and circular discs. Powder Technol. 143144, 2–18.
Shipway, P.H., Hutchings, I.M., 1993a. Fracture of brittle spheres under compression and impact loading. I. Elastic stress distributions. Philos. Mag. A 67 (6), 1389–1404.
Shipway, P.H., Hutchings, I.M., 1993b. Fracture of brittle spheres under compression and impact loading. II. Results for lead-glass and sapphire spheres. Philos. Mag. A 67 (6), 1405–1421.
Sternberg, E., Rosenthal, F., 1952. The elastic sphere under concentrated loads. Journal of Applied Mechanics - Transactions of the ASME 19 (4), 413–421.
Swab, J.J., Yu, J., Gamble, R., Kilczewski, S., 2011. Analysis of the diametral compression method for determining the tensile strength of transparent magnesium aluminate spinel. Int. J. Fract. 172 (2), 187–192.
Tang, C.A., Xu, X.H., Kou, S.Q., Lindqvist, P.A., Liu, H.Y., 2001. Numerical investigation of particle breakage as applied to mechanical crushing Part I: single-particle breakage. Int. J. Rock Mech. Min. Sci. 38 (8), 1147–1162.
Wijk, G., 1978. Some new theoretical aspects of indirect measurements of the tensile strength of rocks. Int. J. Rock Mech. Min. Sci. Geomech. Abstr. 15 (4), 149–160.
Yap, S.F., Adams, M.J., Seville, J.P., Zhang, Z., 2008. Single and bulk compression of pharmaceutical excipients: evaluation of mechanical properties. Powder Technol. 185 (1), 1–10.
Yoshida, M., Ogiso, H., Nakano, S., Akedo, J., 2005. Compression test system for a single submicrometer particle. Rev. Sci. Instrum. 76 (9), 093905.
Zhao, S., Gan, Y., Kamlah, M., Kennerknecht, T., Rolli, R., 2013. Influence of plate material on the contact strength of Li_4sio_4 pebbles in crush tests and evaluation of the contact strength in pebble pebble contact. Eng. Fract. Mech. 100, 28–37. https://www.sciencedirect.com/science/article/pii/S0013794412002135.